coatings

Article

Structural, Magnetic and Gas Sensing Activity of Pure and Cr Doped In$_2$O$_3$ Thin Films Grown by Pulsed Laser Deposition

Veeraswamy Yaragani [1,*,†], Hari Prasad Kamatam [1,2,†], Karuppiah Deva Arun Kumar [3], Paolo Mele [3,*], Arulanandam Jegatha Christy [4], Kugalur Venkidusamy Gunavathy [5], Sultan Alomairy [6] and Mohammed Sultan Al-Buriahi [7]

[1] Department of Physics, Institute of Aeronautical Engineering, Dundigal, Hyderabad 500043, India; k.hariprasad500@gmail.com
[2] Department of Physics, Pondicherry University, Puducherry 605014, India
[3] College of Engineering, Shibaura Institute of Technology, Saitama 337-8570, Japan; i048267@shibaura-it.ac.jp
[4] Department of Physics, Jayaraj Annapackiam College for Women, Periyakulam, Theni 625601, India; jegathachristy@gmail.com
[5] Department of Physics, Kongu Engineering College, Perundurai 638060, India; gunavathy@kongu.ac.in
[6] Department of Physics, College of Science, Taif University, P.O. Box 11099, Taif 21944, Saudi Arabia; mohsaa996@gmail.com
[7] Department of Physics, Sakarya University, 54100 Sakarya, Turkey; mohammed.al-buriahi@ogr.sakarya.edu.tr
* Correspondence: veerayaragani@gmail.com (V.Y.); pmele@shibaura-it.ac.jp (P.M.)
† Author contributed equally.

Abstract: Pure In$_2$O$_3$ and 6% Cr-doped In$_2$O$_3$ thin films were prepared on a silicon (Si) substrate by pulsed laser deposition technique. The obtained In$_2$O$_3$/In$_2$O$_3$:Cr thin films structural, morphological, optical, magnetic and gas sensing properties were briefly investigated. The X-ray diffraction results confirmed that the grown thin films are in single-phase cubic bixbyte structure with space group *I*a-3. The SEM analysis showed the formation of agglomerated spherical shape morphology with the decreased average grain size for Cr doped In$_2$O$_3$ thin film compared to pure In$_2$O$_3$ film. It is observed that the Cr doped In$_2$O$_3$ thin film shows the lower band gap energy and that the corresponding transmittance is around 80%. The X-ray photoelectron spectroscopy measurements revealed that the presence of oxygen vacancy in the doped In$_2$O$_3$ film. These oxygen defects could play a significant role to enhance the sensing performance towards chemical species. In the magnetic hysteresis loop, it is clear that the prepared films confirm the ferromagnetic behaviour and the maximum saturation value of 39 emu/cc for Cr doped In$_2$O$_3$ film. NH$_3$ gas sensing studies was also carried out at room temperature for both pure and Cr doped In$_2$O$_3$ films, and the obtained higher sensitivity is 182% for Cr doped In$_2$O$_3$, which is about nine times higher than for the pure In$_2$O$_3$ film due to the presence of defects on the doped film surface.

Keywords: In$_2$O$_3$/In$_2$O$_3$:Cr thin films; XPS; magnetization property; NH$_3$ sensor

1. Introduction

High carrier mobility with the magnetic property of transparent metal oxides attracts as a miniature robust device for spintronic applications. This class of materials is called diluted magnetic metal oxide semiconductors (DMOS) [1]. These magnetic semiconductors could lead to unite the electrical manipulation of magnetic states and the magnetic adjustment of electrical signals that could result in devices such as bipolar transistors, spin resonant diodes, spin field effect transistors, magnetic semiconductor tunnel junction devices, magnetic bipolar junction diodes, and transistors, etc. [2–8]. If carrier-mediated magnetization can be induced in transparent semiconducting oxides such as In$_2$O$_3$, ZnO, TiO$_2$, etc., it is predicted that such DMOS will exhibit coupling among electrical, optical, and magnetic properties, further boosting the prospects of devices emanating from such materials. Among various transparent conducting oxide materials, In$_2$O$_3$, ZnO and SnO$_2$

are multipurpose materials with a wide range of applications in optoelectronics, solar cells, gas sensors, etc. [9–13], due to the interstitial defects of oxygen and other state defects. In_2O_3 is an n-type semiconductor with high optical bandgap with cubic bixbite crystal structure. Inducing magnetic ordering in In_2O_3 based materials will further enhance its utility in several devices. In the past, a few attempts were made to probe the magnetic properties of transition metal doped In_2O_3. However, the origin of magnetism in such system has been a matter of debate. In those, Philip et al. [14] reported that ferromagnetic ordering in Cr doped In_2O_3 is due to carrier mediation. Jayakumar et al. [15] suggested that defects in the synthesis may cause magnetism in Fe-doped In_2O_3 thin films. Garcia et al. [16] reported that double exchange interaction between metal ions of different valence oxides. According to Chang et al., Mo doped In_2O_3 exhibited good ferromagnetism attributed to the indirect exchange interaction of the charge carriers available in In_2O_3 [17]. Khare et al. discussed the origin of room temperature ferromagnetism in Cr doped In_2O_3 films and they observed that the ferromagnetic behaviour can improve after high vacuum annealing [18]. Ukah et al. described the structural and electrical transport properties of Cr doped In_2O_3 films and they suggested that the pulsed laser deposition technique (PLD) has more advantage than other deposition techniques [19]. From the above discussions, it is evident that the properties of In_2O_3 based DMOS depend on the dopant; and, defects would alter the electronic structure of such materials. However, not much is known about the modification in the electronic structure of In_2O_3 occurring due to such defects or dopants. Probing the electronic structure will be key to understanding the underlying mechanism responsible for the coupled electrical, optical and magnetic properties of In_2O_3 based DMOS and to accordingly design the material for device application. It is also predicted that the transparent semiconducting indium oxide (In_2O_3) based DMOS would exhibit coupling among electrical, optical, and magnetic properties.

In addition, we also investigate the ammonia (NH_3) gas sensing properties of In_2O_3 because of its surface controlled type semiconductor [20], which reacts well with the surrounding chemical species. In the case of metal doped In_2O_3, researchers have mainly focused on magnetic device applications due to the native ferromagnetic properties. In_2O_3 based thin film sensor could be applicable for gas sensing devices due to impurity defects and/or native defects of oxygen vacancies by metal doping and or changing the deposition parameters. Recently, Wang et al. [21] synthesized Co-doped In_2O_3 nanorods for formaldehyde (HCHO) gas sensor. They observed that the increase of response from undoped to doped films is attributed to the doping elements, creating a high surface area which could offer the adsorption of gas molecules and improve the response. Han et al. [22] reported the response of Ce doped In_2O_3 nanospheres towards methanol gas at an operating temperature of 320 °C. They observed the maximum response of ~35 at 100 ppm of methanol for the doped film, which is higher than the pure In_2O_3. Further, they obtained fast response/recovery times (14/10 s) with respect to methanol due to the sensor operating temperature. Manivasaham et al. [23] prepared undoped and Cr doped ZnO films for room temperature NH_3 sensor and obtained the best response for Cr doped ZnO compared to undoped ZnO film. From the above reports, the defects of oxygen play a major role in improving the sensing response towards any chemical species. Among other gases, sensing behaviour is high for ammonia at room temperature. The room temperature sensors have numerous profits such as less complex circuitry, safety in burnable situation, low power consumption, and there is no requirement of any heating circuits, etc.

In this study, we report the structural, magnetic, optical and gas sensing studies of pure In_2O_3 and Cr doped In_2O_3 films fabricated by pulsed laser deposition (PLD). The fabricated In_2O_3/In_2O_3:Cr thin films were characterized by different analytical techniques such as XRD, SEM, EDX, XPS, VSM, UV-visible spectrophotometer, and room temperature NH_3 gas sensor measurements.

2. Materials and Methods

2.1. Pellet Preparation by SSR

A well-sintered pellet of pure In_2O_3 and Cr doped In_2O_3 ($In_{2-x}Cr_xO_3$ ($x = 0.06$)) were prepared by solid state reaction (SSR) technique. The high purity In_2O_3 and Cr_2O_3 powders (acquired from Sigma Aldrich) were taken as starting materials to prepare the $In_{2-x}Cr_xO_3$ ($x = 0.06$) powder sample by solid state reaction. Firstly, the required quantity of both In and Cr oxide powders were mixed together for 5 h in a ball milling setup. Further, the mixed powder was continuously heated in air at 800 °C for 10 h and the prepared high purity In_2O_3 and Cr doped In_2O_3 powders were cold pressed at a 10-ton load with the desired dimensions. Finally, the prepared pellets of 25 mm diameter and 2 mm thickness were sintered at 900 °C for 12 h. The density of the sintered pellets was calculated by an immersion-specific gravity method and the value of relative density in percentage was found to be ∼96%.

2.2. Film Preparation by PLD

In the present investigation, the prepared high density In_2O_3 and Cr doped In_2O_3 pellets were used to fabricate thin films on Si (100) substrate by pulsed laser deposition (PLD) technique (Excimer laser KrF ($\lambda = 248$ nm) source; Lambda Physik COMPex 201 Model, Göttingen, Germany). Prior to the deposition, the native oxide must be removed from the Si substrate. Therefore, we used $HF:H_2O$ (1:10) solution treatment for 2 min and then washed with deionized water thrice. Then, pre-cleaned substrate was dried and cleaned with high pure (99.999%) nitrogen gas before loading into the PLD chamber. Then, the PLD chamber was evacuated to a base vacuum of 10^{-6} Torr. During the deposition, the energy density and pulse repetition rates were adjusted at 2.5 J/cm^2 and 10 Hz, respectively, for all thin films. The detailed experimental conditions are listed in Table 1. Oxygen partial pressure was constantly maintained at 1 mTorr for the entire film deposition. Finally, the prepared films were stored in a desiccator to avoid atmosphere contaminations.

Table 1. PLD experimental conditions for Cr doped In_2O_3 thin films.

Parameters	Conditions
Source	KrF Excimer Laser
Base vacuum	1×10^{-6} Torr
Target to substrate distance	6 cm
Substrate rotation	60 rpm
Substrate temperature	670 °C
Laser wavelength	248 nm
Energy density	2.5 J/cm^2
Pulse repetition rate	10 Hz
Pulse duration	8 ns
Deposition time	15 min

2.3. Characterizations

The structural property of films was carried out using GIXRD (D8-Discover system of M/s Bruker, Billerica, MA, USA) equipped with CuK_α. The X-ray photoelectron spectroscopy (XPS) measurement was performed by Omicron energy analyser (EA-125, Vancouver, BC, Canada) to analyse the chemical compositions. All collected data were normalized. The vibrating sample magnetometer (VSM) (Lake Shore: Model: 7404, Westerville, OH, USA) was performed to investigate the magnetic properties of films. The film morphology was analysed using scanning electron microscope (model-ZEISS, Oberkochen, Germany). The optical transmittance of thin films was recorded in the wavelength range between 300 and 1000 nm using a Shimadzu Solid Spec-3700 DUV UV-visible spectrophotometer (Kyoto, Japan). The ammonia (NH_3) sensing properties of In_2O_3/In_2O_3:Cr thin films were investigated by sensor setup with the help of Keithley Source Meter (model 2450, Tectronix Inc., Beaverton, OR, USA). All the characterizations were carried out at room temperature.

3. Results and Discussion

3.1. Structural Analysis

Figure 1 shows the XRD patterns of the prepared pure In_2O_3 and Cr doped In_2O_3 thin films. The observed X-ray diffraction peaks match with the JCPDS (card No. 06-0416) standard data file of indium oxide (In_2O_3), confirming the formation of cubic bixbyte crystal structure of In_2O_3 with the *Ia-3* space group. No extra characteristic peaks were identified in the films that can be related to any metal chromium, and chromium-based oxide compounds. Pure In_2O_3 and Cr doped In_2O_3 thin films exhibit polycrystalline structure with a strong preferred orientation along (222) plane direction. In addition, the (222) plane peak position was slightly shifted towards the higher angle for Cr doped In_2O_3 thin film attributed to interstitial doping of metallic cations. The lattice parameters are evaluated by analysing the observed XRD patterns of the prepared films using the celref3 software and are found to be 10.11 and 10.12 Å, respectively. The average crystallite size value of pure and Cr doped In_2O_3 thin films were determined using Scherer's equation [24].

$$D = \frac{0.9\,\lambda}{\beta \cos\theta}, \tag{1}$$

where, D is the average crystallite size, β is the full width at half maximum (FWHM) of the diffraction peak, λ is the wavelength of CuK_α radiation, and θ is the Bragg's angle. The calculated average crystallite size values of the pure In_2O_3 and Cr doped In_2O_3 films are found to be 26 and 21 nm, respectively. Clearly, the calculated D value is decreased from undoped to doped In_2O_3 films due to increase of FWHM. Krishna et al. [25] reported the reduction of crystallite size from 40 to 31 nm for pure In_2O_3 and Cr-doped In_2O_3 thin films. The decrease of the D value might be due to the reason that doped Cr ions might disturb the grain growth level of native In-O lattice. From the XRD analysis, it is confirmed that the formation of nanocrystalline cubic bixbyte phase for both pure In_2O_3 and Cr-doped In_2O_3 thin films.
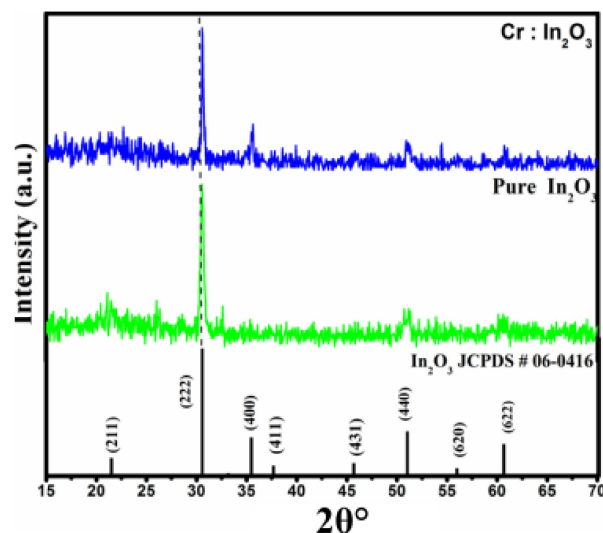

Figure 1. XRD patterns of pure In_2O_3 and Cr doped In_2O_3 thin films with a standard JCPDS file data.

3.2. Surface Morphology Analyses

Figure S1 (Supplementary Materials) shows the SEM micrographs of the fabricated (a) pure In_2O_3 and (c) Cr-doped In_2O_3 thin films, respectively. From the figure, the observed SEM micrographs show the agglomerated spherical shaped grains for both pure and Cr doped In_2O_3 thin films. The average particle (grain) size of pure In_2O_3 and Cr-doped In_2O_3 thin films, respectively, are found to be in the ranges 25–40 nm and 20–35 nm. It is revealed that Cr doped In_2O_3 thin film has less particle size when compared to pure In_2O_3; which is

correlated with XRD results. A lesser particle size could enhance the surface to volume ratio; this offers an appropriate increased surface environment for effective adsorption of surrounding gases. Consequently, there is an increase of the gas sensing response with quick reaction time. Figure S1b,d shows the EDX spectrum of pure In_2O_3 and Cr doped In_2O_3 films, respectively. From Figure S1b, EDX spectrum shows the presence of In and O elements in the pure In_2O_3 thin film. The obtained EDX spectrum confirms the absence of other impurities, which established the purity of the In_2O_3. In Figure S1d, EDX spectrum shows the existence of In, Cr and O elements in the Cr doped In_2O_3 thin film and the absence of other elements. Both pure and doped In_2O_3 films exhibit a high intense peak at 1.8 keV, corresponding to the Si element, which is originated from the substrate.

Figure 2 shows the 2D and 3D AFM images of pure In_2O_3 and Cr doped In_2O_3 thin films. The surface roughness is one of the crucial parameters to understand the sensing performance of metal oxide thin films. As seen from Figure 2a, the pure In_2O_3 film shows spherical grains uniformly arranged on the film surface, whereas, as shown in Figure 2b, the Cr doped film exhibits spherical grains. The average surface roughness values were found to be 9 and 14 nm for pure and Cr doped In_2O_3 films, respectively. In general, the rough film surface performs well in sensing behaviour by attracting more oxygen species from the air and releasing the electron with the interaction between oxygen and the surrounding gases. Among the prepared films, Cr doped In_2O_3 film have a higher surface roughness than that for pure In_2O_3, which might be due to the formation of Cr defects in the host lattice. Therefore, we believe that the doped In_2O_3 film has more useful topographies for enhancing sensing performance.
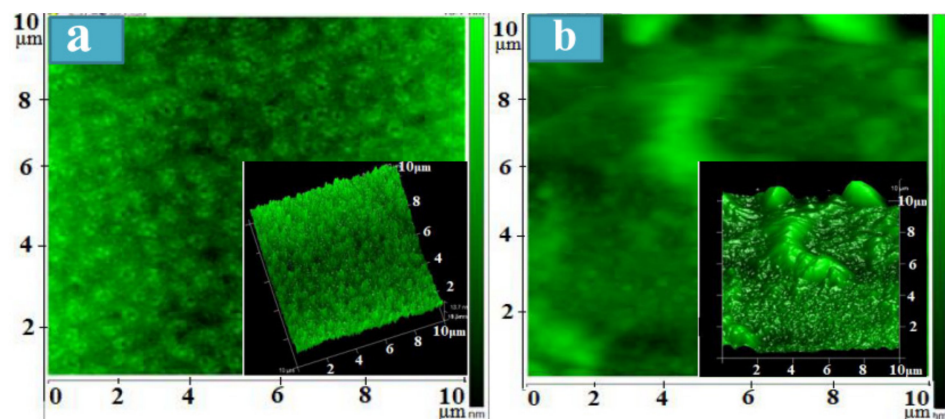

Figure 2. 2D and 3D AFM images of (**a**) pure In_2O_3 and (**b**) Cr doped In_2O_3 thin films.

3.3. Optical Analysis

Figure 3a shows the optical transmittance spectra of pure In_2O_3 and Cr doped In_2O_3 thin films. From the figure, it is clear that both the pure and doped In_2O_3 thin films are highly transparent in the visible region (~80%). The transmittance of Cr doped In_2O_3 film is lower when compared with the pure In_2O_3 film due the presence of Cr impurities. The decrease of transmittance might be due to increase in film thickness by external impurities. A steep absorption edge is originating near the UV region for both films; and, the edge is shifted to a higher wavelength side for the doped In_2O_3 film by absorbing the higher energy photons. This sharp fall near the UV range infers good crystalline nature of the wide bandgap of the prepared films. The optical band gap of the pure and Cr doped In_2O_3 films can be estimated from the relation [26].
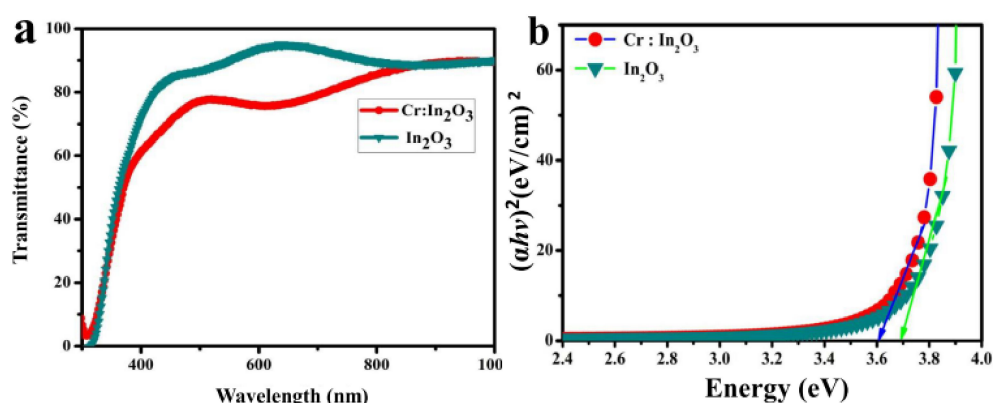
$$\alpha h\upsilon = B\left(h\upsilon - E_g\right)^n \tag{2}$$

Figure 3. (**a**) Optical transmittance and (**b**) bandgap spectra of pure and Cr doped In_2O_3 films.

Optical bandgap of pure In_2O_3 and Cr doped In_2O_3 thin films are assumed from the plot of $(\alpha h\upsilon)^2$ vs. $h\upsilon$, as given in Figure 3b. The direct bandgap (E_g) values of pure and Cr doped In_2O_3 thin films were found to be decreased from 3.69 to 3.61 eV. Habib et al. [27] observed the decrease of bandgap from pure to Cr doped metal oxide thin films due to the formation of defects and/or the higher flow of electrons between valence band to the conduction band.

The observed lower bandgap value of Cr doped In_2O_3 thin film is attributed to the lower crystallite size obtained from XRD. In addition, the change of bandgap might be due to the influence of various factors such as particle size, doping impurities, carrier concentration, and deviation of elemental stoichiometry in the crystal lattice. In our case, there is a reduction of crystallite size, which causes the decrease of bandgap from pure to doped films.

3.4. X-ray Photoelectron Spectroscopy Analysis

Figure 4a shows the X-ray photoelectron survey scan spectrum of the Cr doped In_2O_3 thin film. The detailed survey scan spectrum has been performed to determine the ionic state of Indium (In), Chromium (Cr), and Oxygen (O) in the deposited Cr doped In_2O_3 thin film. From Figure 4a, there are several peaks observed related to the presence of different electronic states of In, Cr, and O.
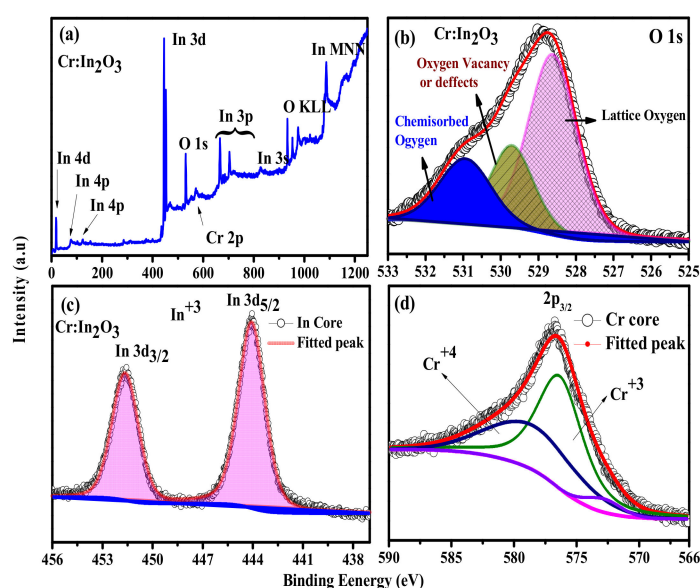

Figure 4. X-ray photoelectron spectra of (**a**) survey scan, (**b**) oxygen core level (**c**) indium core level and (**d**) chromium core level for the Cr doped In_2O_3 thin film.

Figure 4b shows the observed core level fine spectra of O 1s from the Cr doped In_2O_3 thin film. From Figure 4b, the deconvolution of the observed spectrum shows the presence of three distinguished peaks. The high intense peak exhibited at 528.4 eV related to the lattice oxygen, while the other higher binding energy peak at 531.2 eV is due to the presence of adsorbed oxygen on the film surface [21]. The centre peak located at 529.6 eV is due to the presence of oxygen vacancy in the film surface. Oxygen vacancy in the film is rather a familiar occurrence in transparent oxide films due to the loss of oxygen during the synthesis process. The presence of the oxygen vacancy state can be understood from the Cr core-level spectrum. In Figure 4c, it is observed that In (3d) core-level spectrum contains two peaks and the spin-orbit splitting is 7.6 eV in-between two peaks. Features of In-3d core-level spectrum are fitted with combined Gaussian function and the observed peaks corresponding to $In-3d_{3/2}$ and $In-3d_{5/2}$ states are observed at 451.6 and 444 eV, respectively [28]. These are consistent with the 3^+ state of indium (In) in In_2O_3 lattice. A similar spectrum was also observed for the pure In_2O_3 thin film.

Figure 4d shows the Cr $2p_{3/2}$ core level spectrum of Cr doped In_2O_3 thin film. The spectrum was corrected with Shirley background approximation and fitted with the combined Gaussian function. The fitted spectrum reflects the presence of Cr^{3+} state along with the Cr^{4+} state. The most intense peak at 576.3 eV is assigned as Cr^{3+} state and a hump at higher energy tail of Cr^{3+} state reflects the presence of higher oxidation state Cr^{4+}. The hump cannot be a satellite feature due to Cr^{3+} state since its position should appear at 11 eV higher in binding energy from the Cr $2p_{3/2}$ feature. A small feature of 572.7 eV is due to the multiple splitting of Cr 2p energy levels [29]. The occurrence of 3^+ and 4^+ states of Cr ions suggest its substitutional character and excludes the possibility of Cr clusters in the studied film. The hetero-valency of Cr ion can be explained by the occurrence of oxygen vacancy from the prepared film.

3.5. VSM Analysis

Figure 5 shows the magnetization vs. the applied magnetic field (M-H) curves of pure In_2O_3 and Cr doped In_2O_3 thin films measured at room temperature. The magnetization data of both the films were rectified by subtracting the effect of substrate contribution. From Figure 5, it is observed that the prepared films exhibit a tolerant ferromagnetism with an increase of saturation magnetization (M_s). It is a well-known fact that the pure In_2O_3 thin film exhibits ferromagnetic behaviour with lower M_s value when compared to a diamagnetic nature of stoichiometric bulk In_2O_3 [25]. This weak ferromagnetism of the In_2O_3 thin film might be due to the presence of some anion vacancies in the film [7]. From Figure 5, it is observed that Cr-doped In_2O_3 thin film shows higher saturation magnetization (M_s) value when compared to the pure In_2O_3 thin film due to the incorporation of Cr into the host lattice. The increase in saturation magnetic moment from pure In_2O_3 (23 emu/cc) to Cr doped In_2O_3 (39 emu/cc) thin films is at 10,000 (Oe). This may be due to the magnetic exchange between Cr^{3+} and In^{3+} around free electron trapped sites and also the oxygen vacancies along with trapped electrons, which leads to enhance the ferromagnetic behaviour. It is also clear that the Cr doped In_2O_3 thin film exhibits good ferromagnetism; though, the saturation magnetization value remains very close to pure In_2O_3. This fundamental ferromagnetism may be occurring from the magnetic exchange interactions of the trapped electrons in the anionic vacancies called as F-centred mediated ferromagnetism. This mechanism is extensively presumed to be the origin of ferromagnetism in metal oxide thin films as well as a DMS system. Therefore, we believe that such an F-centre mediated ferromagnetism occurs in our prepared film because of the vacuum deposited Cr doped In_2O_3 film, which leads to the creation of oxygen vacancies. Such oxygen vacancies can trap the free electrons, as described by Coey et al. [30], and these trapped electrons act as F-centres. These F-centres mediate and could lead to a magnetic exchange interaction process in the neighbouring metal cations.
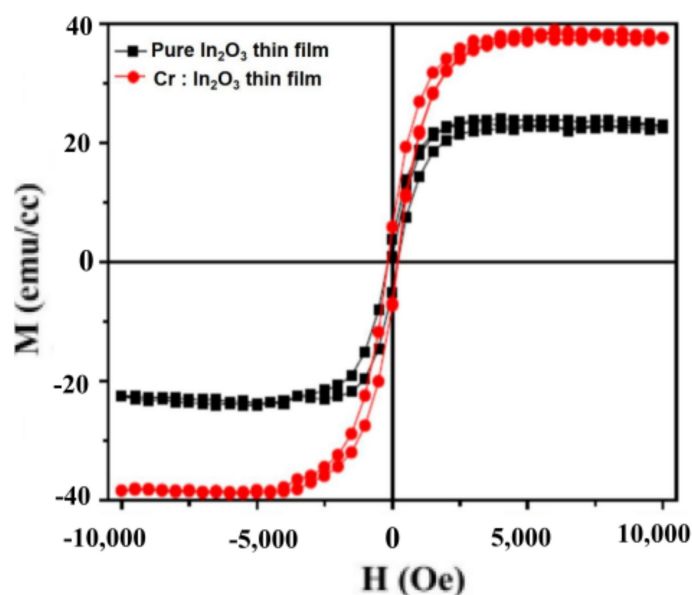
Figure 5. M-H curves of pure In_2O_3 and Cr doped In_2O_3 thin films measured at room temperature.

3.6. Ammonia (NH_3) Sensing Studies

The room temperature NH_3 sensing properties of the prepared pure In_2O_3 and Cr doped In_2O_3 films were studied using home-made gas sensing setup (Figure 6). The gas sensing response is mainly dependent on the surface morphology, operating temperature, and metal doping for metal oxide materials. Amongst them, the operating temperature plays a key role in improving the sensor's gas sensitivity because it controls the electrical resistivity by changing the activation energy. Han et al. [22] and Wang et al. [21] reported that the sensitivity of In_2O_3 is increased with the increasing operating temperature due to decrease in the activation energy and the molecular motion acceleration. However, scientists are focusing on improving its sensitivity at room temperature to ensure a safe and nontoxic environment in medical laboratories and chemical industries. [31]. In view of this, the performance of room temperature ammonia sensor for different NH_3 concentrations is reported in the present study.
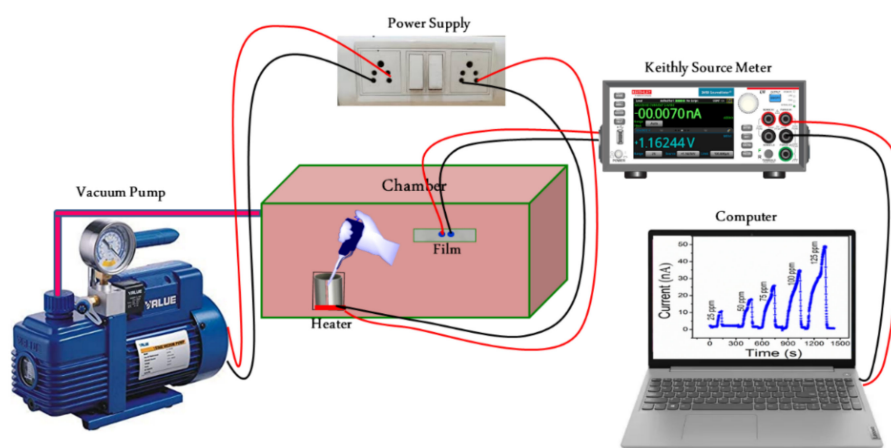

Figure 6. Schematic diagram of the ammonia gas sensing setup.

3.6.1. Sensitivity

The electrical current deviation of pure In_2O_3 and Cr doped In_2O_3 films were measured with different NH_3 concentrations, such as 25, 50, 75, 100, and 125 ppm, and are shown in Figure 7. It is observed that the base current (under air) value is slightly decreased from

pure In_2O_3 (2.21×10^{-9} A) to Cr doped In_2O_3 film (1.01×10^{-9} A). This may possibly be due to suppression of the electron carrier concentration of host In_2O_3 lattice by the presence of surface defects of oxygen. Caricato et al. [32] observed the reduction of both mobility and carrier concentration when Cr metal doping into the ITO film. However, for the gas sensor applications, the surface related oxygen defects can enhance the sensing response by chemical reaction of both film surface and chemical species. As seen in Figure 7, the electrical current was significantly increased when increasing NH_3 concentrations for both pure and Cr doped In_2O_3 film sensors. This is because of more electrons moving to the conduction band once the NH_3 species interact with the surface of In_2O_3 film. When compared to pure In_2O_3, the current level reaches a maximum for Cr doped In_2O_3 film due to more surface defects by Cr inclusion.
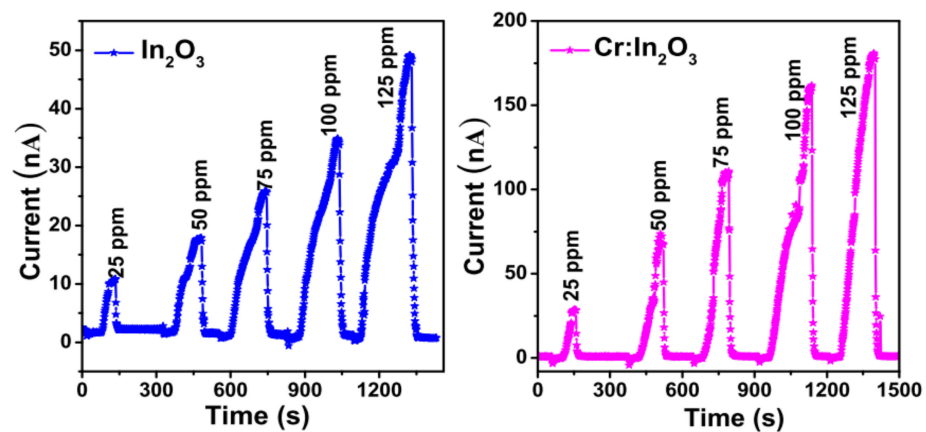

Figure 7. Electrical current variation of pure In_2O_3 and Cr doped In_2O_3 thin films at different NH_3 concentration (ppm).

From the observed current value under air and NH_3 atmosphere conditions, the gas sensitivity was calculated by using the following equation [31],

$$S = \frac{(I_g - I_a)}{I_a} \qquad (3)$$

where, I_g is the electrical current at gas atmosphere and I_a is the electrical current at air atmosphere. Figure 8 illustrates the sensitivity variation of pure and Cr doped In_2O_3 films with respect to NH_3 concentrations. It can be seen from the figure that the pure In_2O_3 film show a less sensitivity of 4% and then it reaches up to 28% (at 25 ppm of NH_3), while Cr is included in the In_2O_3 film. This can be explained on the change of surface activity and structural disorder by doping. Both XRD and AFM results evidenced that there is a decrease in the crystallite size and increase in the surface roughness for Cr doped In_2O_3 film compared to the pure In_2O_3. Due to having high surface roughness and/or large surface area, higher number of NH_3 molecules are adsorbed on the In_2O_3 film surface, which generates more oxygen ions, resulting in enhancement of the sensitivity. Moreover, it is noticed that the sensing response is steadily increased from 21% to 182% at 125 ppm of NH_3 for pure and Cr doped In_2O_3 films. The following reasons can be considered for the increase of sensitivity; (i) increase of the surface catalytic effect on the In_2O_3 surface caused by NH_3 adsorption (ii) the adsorbed oxygen ions heavily interact with more NH_3 species, (iii) the rate of combustion reaction between film surface and the testing gas is increased by increase in NH_3 concentration due to low activation energy. Hassan et al. [33] reported the increase of sensing response from the undoped ZnO to Cr doped ZnO thin films by the presence of oxygen defects in the host structure.
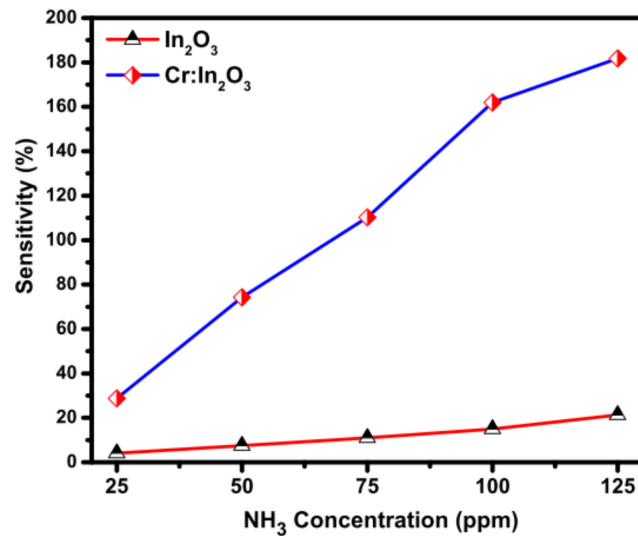
Figure 8. Variation of NH$_3$ sensitivity for pure In$_2$O$_3$ and Cr doped In$_2$O$_3$ thin films at different NH$_3$ concentrations.

3.6.2. Response and Recovery Speed

Response and recovery times are the key parameters for gas sensor applications. In general, the metal oxide-based sensor should be having a faster response and recovery time with respect to chemical species due to the adsorption of more oxygen ions on the film surface. The required time taken to reach 90% of the current is known as response time and the exact inverse trend is known as recovery time. Figure 9a illustrates the plot of response and recovery times for pure In$_2$O$_3$ thin film at 25 ppm of NH$_3$. The observed response and recovery times increase with increase of NH$_3$ concentration, as given in Figure 9b. This may be attributed to increasing the interaction rate of adsorbed oxygen and NH$_3$ species, and therefore, releasing electrons to the conduction band of host lattice. The obtained recovery time is less when compared to response time because the chemisorbed oxygen ions are taking lesser time to desorb from the film surface. In the present work, the observed response time is 28 s, and the corresponding recovery time is 6 s for Cr doped In$_2$O$_3$ film at 25 ppm. Hassan et al. [33] obtained the least response and recovery times, which are 15 and 72 s, respectively, for Cr doped ZnO thin film. Han et al. [22] reported response/recovery times of 14/10 s for Ce doped In$_2$O$_3$ nanospheres. In our case, both the values are nearly the same as the above reported values.
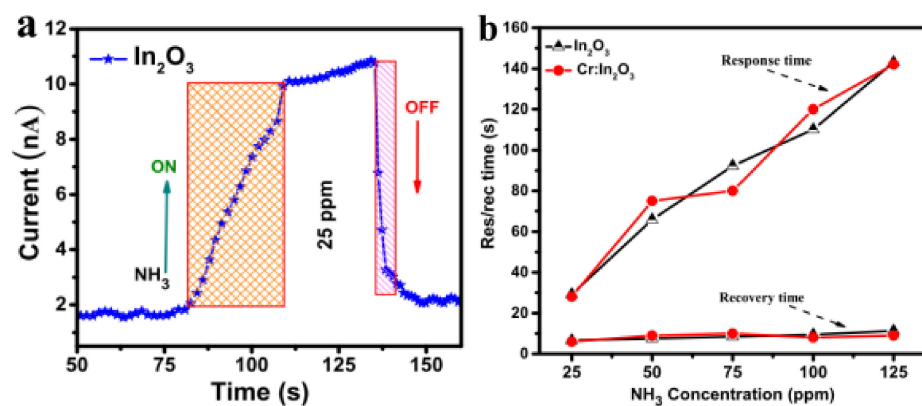

Figure 9. (**a**) Plot of response/recovery time at 25 ppm for pure In$_2$O$_3$, (**b**) variation of response and recovery times for pure and doped films with respect to different NH$_3$ concentrations.

3.6.3. Sensing Mechanism of NH_3/In_2O_3

In_2O_3 is one of the familiar semiconducting n-type sensing materials because of its surface-controlled type. The gas sensing performance of In_2O_3 sensor with respect to analyte gas can be explained by the changing in current upon exposure to different gas concentrations. Oxygen ions and its related defects play a key role in enhancing the sensing response, therefore, its necessary to understand both adsorption and desorption of oxygen ions under air and surrounding gas atmosphere. When the In_2O_3 film is exposed in air atmosphere, the electrical current is suppressed by the adsorbed O_2 molecules, which are converted as negative charged oxygen ions (O_2^-, O^- or O^{2-}) by extracting the electrons from the conduction band (CB). At room temperature, O_2^- ionized oxygen is formed in the prepared In_2O_3 film surface. Due to the creation of O_2^- ions, a depletion layer is formed. As a result, an initial low electrical current is observed. The formation of negatively charged O_2^- ions on the film surface can be written as $O_{2(ads)} + e \rightarrow O_2^-$ [34]. Under NH_3 atmosphere, the film surface reacts with chemical spices and releases the captured electrons back into the *CB*. Consequently, there is an increase in carrier concentrations. Therefore, the electron depletion layer becomes thin and can be described as $4NH_{3(ads)} + 2O^-_{(ads)} \rightarrow N_{2(ads)} + 6H_2O_{(ads)} + 2e^-$. The observed NH_3 performance can possibly be explained by the following reasons: (i) The higher surface roughness of Cr doped In_2O_3 provides fast chemisorb reaction and accelerates the negative charged ions, which leads to an increase in the sensing response, (ii) the incorporation of Cr^{3+} ions act as a donor by replacing In^{3+}, consequently, it can improve the oxygen vacancies, which leads to enhancement of sensitivity.

3.6.4. Relative Humidity (RH) and Repeatability

Relative humidity (RH) analysis is one of the major parameters to investigate the performance of NH_3 humidity for the pure and Cr doped In_2O_3 films at room temperature. Initially, In_2O_3 film was exposed to NH_3 at 125 ppm under various humidity conditions such as 33%, 54%, and 75%, which are found from the saturated solutions NaCl, $MgCl_2$, and $Mg(NO_3)_2$. Figure S2 (Supplementary File) shows the observed current variation with respect to time for both pure and Cr doped In_2O_3 films. Here, the saturated solutions NaCl, $MgCl_2$, $Mg(NO_3)_2$ are labelled as RH_1, RH_2, and RH_3, respectively, as given in Figure S2. Under humidity air condition, the H_2O molecules could be adsorbed on the In_2O_3 film surface, it converts a hydroxyl form and thus donates the electrons to the In_2O_3 lattice. Further, the adsorbed H_2O molecules can replace the oxygen ions in the film surface and create the electrons to the conduction band. Due to the above reasons, there is an increase of electron carrier concertation as well as electrical current as seen in Figure S2. The figure shows the reduction of electrical current on increasing relative humidity in percentage. This might be due to the H_2O molecules being directly chemisorbed on the oxygen vacancy sites [35]. Pandeeswari et al. [36] suggested the reduction of response being due to the hydrophobic nature of the film.

Repeatability of the pure In_2O_3 and Cr doped In_2O_3 films were accomplished for five consecutive cycles using 25 ppm of NH_3 are, which are given in Figure 10. The figure shows that the observed current level is maintaining the same range for all five cycles. Additionally, it is maintaining a fast response and recovery times towards 25 ppm of NH_3 species. Hence, we conclude that the prepared In_2O_3/In_2O_3:Cr films based metal oxide sensor has good repeatability and can be used in commercial sensors.
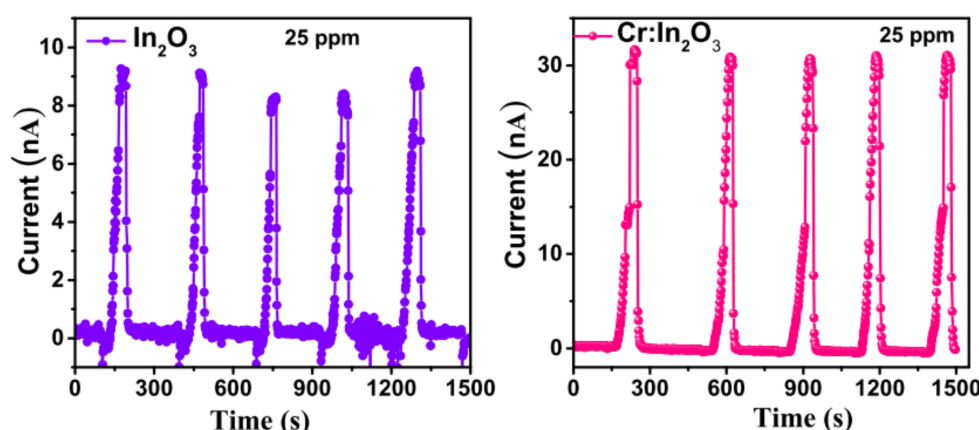
Figure 10. Repeatability for both pure In_2O_3 and Cr doped In_2O_3 thin films at 25 ppm of NH_3.

4. Conclusions

In summary, the successful fabrication of In_2O_3 and Cr-doped In_2O_3 thin films onto a Si substrate by PLD technique is reported in this article. The deposited films are crystalline and grown in a single phase without any impurity, which is confirmed by the XRD studies. The XPS analysis highlights that Cr doped In_2O_3 thin film has oxygen vacancies, which also lead to mixed oxidations states of Cr in 3^+ and 4^+ states. A decrease in the bandgap value from pure to doped In_2O_3 films is due to the existence of defects by Cr doping. The Cr doped In_2O_3 thin film sensor showed a maximum sensitivity of 182% at 125 ppm of NH_3 due to good material properties such as high surface roughness and defects of oxygen. Both AFM and XPS results support the enhancement of sensitivity from pure to Cr doped In_2O_3 thin film sensor. The doped In_2O_3 sensor also exhibits fast response and recovery times of 28 and 6 s respectively. The prepared In_2O_3/In_2O_3:Cr films have good repeatability; therefore, we propose that In_2O_3 based sensor could be used in commercial sensor devices.

References

1. Bader, S.D.; Parkin, S.S.P. Spintronics. *Annu. Rev. Condens. Matter Phys.* **2010**, *1*, 71–88. [CrossRef]
2. Datta, S.; Das, B. Electronic analog of the electro-optic modulator. *Appl. Phys. Lett.* **1990**, *56*, 665–667. [CrossRef]
3. Miwa, S.; Ishibashi, S.; Tomita, H.; Nozaki, T.; Tamura, E.; Ando, K.; Mizuochi, N.; Saruya, T.; Kubota, H.; Yakushiji, K.; et al. Highly sensitive nanoscale spin-torque diode. *Nat. Mater.* **2013**, *13*, 50–56. [CrossRef] [PubMed]

4. Žutić, I.; Fabian, J.; Das Sarma, S. Spintronics: Fundamentals and applications. *Rev. Mod. Phys.* **2004**, *76*, 323–410. [CrossRef]
5. Ertler, C.; Fabian, J. Resonant tunneling magnetoresistance in coupled quantum wells. *Appl. Phys. Lett.* **2006**, *89*, 242101. [CrossRef]
6. Yoo, J.W.; Chen, C.Y.; Jang, H.W.; Bark, C.W.; Prigodin, V.N.; Eom, C.B.; Epsteinn, A.J. Erratum: Spin injection/detection using an organic-based magnetic semiconductor. *Nat. Mater.* **2010**, *9*, 778. [CrossRef]
7. Watanabe, S.; Ando, K.; Kang, K.; Mooser, S.; Vaynzof, Y.; Kurebayashi, H.; Saitoh, E.; Sirringhaus, H. Polaron spin current transport in organic semiconductors. *Nat. Phys.* **2014**, *10*, 308–313. [CrossRef]
8. Boales, J.A.; Boone, C.T.; Mohanty, P. Nanomechanical detection of the spin Hall effect. *Phys. Rev. B* **2016**, *93*, 161414. [CrossRef]
9. Hamberg, I.; Granqvist, C.G. Evaporated Sn-doped In_2O_3 films: Basic optical properties and applications to energy-efficient windows. *J. Appl. Phys.* **1986**, *60*, R123–R160. [CrossRef]
10. Odaka, H.; Iwata, S.; Taga, N.; Ohnishi, S.; Kaneta, Y.; Shigesato, Y. Study on electronic structure and optoelectronic properties of indium oxide by first-principles calculations. *Jpn. J. Appl. Phys.* **1997**, *36*, 5551–5554. [CrossRef]
11. Ginley, D.S.; Bright, C. Transparent conducting oxides. *MRS Bull.* **2000**, *25*, 15–18. [CrossRef]
12. Kumar, K.D.A.; Mele, P.; Ponraj, J.S.; Haunsbhavi, K.; Varadharajaperumal, S.; Alagarasan, D.; Algarni, H.; Angadi, B.; Murahari, P.; Ramesh, K. Methanol solvent effect on photosensing performance of AZO thin films grown by nebulizer spray pyrolysis. *Semicond. Sci. Technol.* **2020**, *35*, 085013. [CrossRef]
13. Batzill, M.; Diebold, U. The surface and materials science of tin oxide. *Prog. Surf. Sci.* **2005**, *79*, 47–154. [CrossRef]
14. Philip, J.R.; Punnoose, A.; Kim, B.I.; Reddy, K.M.; Layne, S.P.; Holmes, J.; Satpati, B.; LeClair, P.; Santos, T.S.; Moodera, J.S. Carrier-controlled ferromagnetism in transparent oxide semiconductors. *Nat. Mater.* **2006**, *5*, 298–304. [CrossRef] [PubMed]
15. Jayakumar, O.D.; Gopalakrishnan, I.K.; Kulshreshtha, S.K.; Gupta, A.; Rao, K.V.; Louzguine-Luzgin, D.V.; Inoue, A.; Glans, P.-A.; Guo, J.; Samanta, K.; et al. Structural and magnetic properties of $(In_{1-x}Fe_x)_2O_3$ $(0.0 \leq x \leq 0.25)$ system: Prepared by gel combustion method. *Appl. Phys. Lett.* **2007**, *91*, 052504. [CrossRef]
16. Garcia, M.A.; Ruiz-González, M.L.; Quesada, A.; Costa-Kramer, J.L.; Fernandez, J.F.; Khatib, S.J.; Wennberg, A.; Caballero, A.C.; Martín-González, M.S.; Villegas, M.; et al. Interface Double-Exchange Ferromagnetism in the Mn-Zn-O System: New Class of Biphase Magnetism. *Phys. Rev. Lett.* **2005**, *94*, 217206. [CrossRef] [PubMed]
17. Chang-Yup, P.; Chun-Yeol, Y.; Kun-Rok, J.; Sung, C.S. Charge-carrier mediated ferromagnetism in Mo-doped In_2O_3 films. *Appl. Phys. Lett.* **2012**, *100*, 222409.
18. Kharel, P.; Sudakar, C.; Sahana, M.B.; Lawes, G.; Suryanarayanan, R.; Naik, R.R.; Naik, V.M. Room temperature ferromagnetism in Cr-doped In_2O_3 on high vacuum annealing of thin films and bulk samples. *J. Appl. Phys.* **2007**, *101*, 09H117. [CrossRef]
19. Ukah, N.; Gupta, R.; Kahol, P.; Ghosh, K. Influence of oxygen growth pressure on laser ablated Cr-doped In_2O_3 thin films. *Appl. Surf. Sci.* **2009**, *255*, 9420–9424. [CrossRef]
20. Xu, J.; Han, J.; Zhang, Y.; Sun, Y.; Xie, B. Studies on alcohol sensing mechanism of ZnO based gas sensors. *Sens. Actuators B Chem.* **2008**, *132*, 334–339. [CrossRef]
21. Wang, Z.; Hou, C.; De, Q.; Gu, F.; Han, D. One-step synthesis of Co-doped In_2O_3 nanorods for high response of formaldehyde sensor at low temperature. *ACS Sens.* **2018**, *3*, 468–475. [CrossRef] [PubMed]
22. Han, D.; Song, P.; Zhang, S.; Zhang, H.; Xu, Q.; Wang, Q. Enhanced methanol gas-sensing performance of Ce-doped In_2O_3 porous nanospheres prepared by hydrothermal method. *Sens. Actuators B Chem.* **2015**, *216*, 488–496. [CrossRef]
23. Manivasaham, A.; Ravichandran, K.; Subha, K. Light intensity effects on the sensitivity of ZnO:Cr gas sensor. *Surf. Eng.* **2017**, *33*, 866–876. [CrossRef]
24. Kumar, K.D.A.; Valanarasu, S.; Ganesh, V.; Shkir, M.; Kathalingam, A.; AlFaify, S. Effect of precursors on key opto-electrical properties of successive ion layer adsorption and reaction-prepared Al:ZnO thin films. *J. Electron. Mater.* **2018**, *47*, 1335–1343. [CrossRef]
25. Krishna, N.S.; Kaleemulla, S.; Amarendra, G.; Rao, N.M.; Krishnamoorthi, C.; Omkaram, I.; Reddy, D.S. Structural, optical and magnetic properties of Cr doped In_2O_3 powders and thin films. *J. Mater. Sci. Mater. Electron.* **2015**, *26*, 8635–8643. [CrossRef]
26. Anand, V.; Sakthivelu, A.; Kumar, K.D.A.; Valanarasu, S.; Ganesh, V.; Shkir, M.; AlFaify, S.; Algarni, H. Rare earth Eu^{3+} co-doped AZO thin films prepared by nebulizer spray pyrolysis technique for optoelectronics. *J. Sol-Gel Sci. Technol.* **2018**, *86*, 293–304. [CrossRef]
27. Habib, I.Y.; Tajuddin, A.A.; Noor, H.A.; Lim, C.M.; Mahadi, A.H.; Kumara, N.T.R.N. Enhanced Carbon monoxide-sensing properties of Chromium-doped ZnO nanostructures. *Sci. Rep.* **2019**, *9*, 1–12. [CrossRef]
28. Beena, D.; Lethy, K.; Vinodkumar, R.; Pillai, V.M.; Ganesan, V.; Phase, D.; Sudheer, S. Effect of substrate temperature on structural, optical and electrical properties of pulsed laser ablated nanostructured indium oxide films. *Appl. Surf. Sci.* **2009**, *255*, 8334–8342. [CrossRef]
29. Tripathi, M.; Choudhary, R.J.; Phase, D.M. Phase coexistence and the magnetic glass-like phase associated with the Morin type spin reorientation phase transition in $SmCrO_3$. *RSC Adv.* **2016**, *6*, 90255–90262. [CrossRef]
30. Coey, J.M.D.; Venkatesan, M.; Fitzgerald, C.B. Donor impurity band exchange in dilute ferromagnetic oxides. *Nat. Mater.* **2005**, *4*, 173–179. [CrossRef]
31. Kumar, K.D.A.; Valanarasu, S.; Ponraj, J.S.; Fernandes, B.J.; Shkir, M.; AlFaify, S.; Murahari, P.; Ramesh, K. Effect of Er doping on the ammonia sensing properties of ZnO thin films prepared by a nebulizer spray technique. *J. Phys. Chem. Solids* **2020**, *144*, 109513. [CrossRef]

32. Caricato, A.P.; Cesaria, M.; Luches, A.; Martino, M.; Maruccio, G.; Valerini, D.; Catalano, M.; Cola, A.; Manera, M.G.; Lomascolo, M.; et al. Electrical and optical properties of ITO and ITO/Cr-doped ITO films. *Appl. Phys. A* **2010**, *101*, 753–758. [CrossRef]

33. Hassan, M.M.; Khan, W.; Mishra, P.; Islam, S.; Naqvi, A. Enhancement in alcohol vapor sensitivity of Cr doped ZnO gas sensor. *Mater. Res. Bull.* **2017**, *93*, 391–400. [CrossRef]

34. Xia, H.; Wang, Y.; Kong, F.; Wang, S.; Zhu, B.; Guo, X.; Zhang, J.; Wu, S. Au-doped WO_3-based sensor for NO_2 detection at low operating temperature. *Sens. Actuators B Chem.* **2008**, *134*, 133–139. [CrossRef]

35. Santhosam, A.J.; Ravichandran, K.; Ahamad, T. Donated free electrons induced enhancement in the NH3 sensing ability of ZnO thin films—Effect of terbium loading. *Sens. Actuators A Phys.* **2020**, *316*, 112376. [CrossRef]

36. Pandeeswari, R.; Jeyaprakash, B. High sensing response of β-Ga2O3 thin film towards ammonia vapours: Influencing factors at room temperature. *Sens. Actuators B Chem.* **2014**, *195*, 206–214. [CrossRef]